

Original article

Imbibition oil recovery from tight reservoir cores using microemulsion: Experiment and simulation

Qinzhi Li¹, Yiwen Wang^{1,2}, Bing Wei¹^{*}, Lele Wang¹, Jun Lu², Jinyu Tang³

¹State Key Laboratory of Oil and Gas Reservoir Geology and Exploitation, Southwest Petroleum University, Chengdu 610500, P. R. China

²McDougall School of Petroleum Engineering, The University of Tulsa, Oklahoma 74104, USA

³Department of Chemical and Petroleum Engineering, United Arab Emirates University, Al Ain 00000, United Arab Emirates

Keywords:

Imbibition
microemulsion
tight reservoir
numerical simulation

Cited as:

Li, Q., Wang, Y., Wei, B., Wang, L., Lu, J., Tang, J. Imbibition oil recovery from tight reservoir cores using microemulsion: Experiment and simulation. *Capillarity*, 2024, 10(2): 38-47.

<https://doi.org/10.46690/capi.2024.02.02>

Abstract:

Despite the promising results obtained from the utilization of interfacial-active additives in enhancing imbibition-based oil recovery from tight reservoirs, the predominant mechanisms governing this process remain inadequately understood. In this work, a meticulously designed workflow is implemented to conduct experiments and modeling focusing on imbibition tests performed on tight sandstone cores while utilizing surfactant and microemulsion. Our primary objective is to investigate the response of oil recovery to these additives and to develop a robust and reliable model that incorporates the intricate interactions, thereby elucidating the underlying mechanisms. Two imbibition fluids are designed, namely, surfactant and microemulsion. A comprehensive investigation is performed to analyze the physicochemical properties of these fluids, encompassing phase behavior, density, viscosity, and wettability alteration, with the aim of establishing fundamental knowledge in the field. Three imbibition tests are carried out to observe the response of oil production and optimize the experimental methodology. A numerical model is developed that fully couples the evolution of relative permeability and capillary pressure with the dynamic processes of emulsification, solubilization and molecular diffusion. The results demonstrate the crucial role of emulsification/solubilization in the imbibition process.

1. Introduction

Unconventional oil and gas resources, especially tight/shale oil, have emerged as an increasingly popular field in global exploration and development, exerting a profound impact on the global energy landscape. For instance, the US shale revolution has facilitated energy independence and transformed the country into a net exporter of oil and gas (Saravanan and Keerthana, 2017). In 2018, the US achieved a crude oil production of 748 million tons, making it the world's leading oil producer. Tight oil accounted for up to 44% of this production, which has become a pivotal factor influencing the global crude oil market's supply-demand dynamics (Zhang et al., 2015). However, unlike conventional reservoir

development techniques, the exploitation of tight/shale oil reservoirs requires hydraulic fracturing to achieve commercial viability. Production from horizontal wells in these reservoirs generally encounters rapid decline, with a short elastic energy development cycle and low crude oil recovery. Consequently, the concept of enhanced oil recovery is continuously emphasized throughout the extraction process. Imbibition has been utilized extensively in the development of various reservoirs to enhance oil recovery. Spontaneous imbibition is the process whereby wetting-phase fluids are propelled into a porous medium by capillary forces, displacing non-wetting-phase fluids (Mason and Morow, 2013; Lin et al., 2016). It serves as a vital mechanism for facilitating the exchange of materials between a dense matrix and a fracture. In the

case of oil-wet reservoirs, capillary forces pose resistance and gravitational forces are relatively weak, resulting in limited imbibition performance (Lu et al., 2014; Ma et al., 2022). However, through mechanisms such as rock surface adsorption and ion-pair desorption, surfactant molecules can transform the nature of the rock surface from lipophilic to hydrophilic, thus intensifying the capillary force-dominated imbibition (Cao et al., 2020; Cai et al., 2022; Zhou et al., 2023). This in turn leads to a reduction in oil-water interfacial tension and a substantial enhancement in oil recovery. In recent years, extensive research has focused on the imbibition behavior in tight/shale reservoirs characterized by complex pore structures (Liang et al., 2021; Pi et al., 2023). The primary control factors of imbibition have been studied through theoretical analysis, physical simulation and numerical modeling. Cai et al. (2012) proposed an analytical model for imbibition in fractal porous media while both considering capillary force and gravity, then Cai et al. (2021) further modified the Lucas-Washburn equation to various micro-channels and porous media. Kathel and Mohanty (2013) performed experimental evaluations of surfactant imbibition in fractured reservoirs with lipophilic partial wettability at the reservoir temperature and salinity. The findings revealed that anionic surfactants containing a high concentration of ethoxylate effectively altered the wettability, resulting in imbibition recovery rates of up to 68% in tight oil-wet sandstone reservoirs. Chen and Mohanty (2013) investigated the mechanism of surfactants in enhancing recovery from fractured oil-wet carbonates through experiments and numerical simulations. Their study demonstrated that surfactants capable of altering wettability and reducing interfacial tension have synergistic effects on oil recovery through imbibition in oleophilic carbonates. Neog and Schechter (2016) examined the impact of surfactant addition to fracturing fluids on imbibition recovery from Wolfcamp shale cores, and the experimental results showed that the system with higher interfacial tension recovered oil more efficiently when the two surfactants had comparable wettability alteration capabilities. Bu et al. (2022) investigated the effect of surfactants on imbibition while accounting for adsorption, diffusion, capillary forces, and relative permeability. The results highlighted the importance of surfactant-induced interfacial tension reduction for enhanced oil recovery and the role of interfacial tension reduction in facilitating gravity drainage. Cheng et al. (2018) utilized Eclipse to construct a core-scale model for simulating surfactant spontaneous imbibition. Their study demonstrated that optimal interfacial tension could exist for different degrees of wettability alteration, and increasing the degree of wettability modification leads to higher oil recovery. Despite these investigations, no consensus has been reached regarding the relationship between interfacial tension, wettability and imbibition behavior. Research on the imbibition mechanisms of systems with ultra-low interfacial tension (IFT) is still in its early stage. Li et al. (2017) studied the imbibition behavior of an ultra-low IFT system in oil-wet carbonate rocks. Surfactant formulations were screened using microemulsion (ME) phase behavior tests and high oil recovery was observed at ultra-low IFT. Buoyancy and horizontally oriented pressure gradients were suggested as the driving forces for imbibition at ultra-low

IFT. Tagavifar et al. (2019) examined the imbibition kinetics of emulsions/MEs at ultra-low IFT and found that spontaneous imbibition is accompanied by a phase transition and rapid formation of MEs. Experimental and simulation results both confirmed that at ultra-low IFT, the sequential processes of solubilization, desaturation of the initial wetting phase and complete wettability transition occur. The kinetic behavior of the imbibition process can be described more accurately if the combined effects of ME formation and wettability transition on fluid flow and surfactant molecular transport are considered. Mejia et al. (2019) investigated the microscopic mechanism of surfactant displacement of the oil phase from lipophilic porous media and found that during imbibition, IFT reduction and ME formation occur more rapidly than wettability changes. The ultra-low IFT significantly reduces the impact of capillary pressure. Liu et al. (2020) studied the effect of spontaneous emulsification on oil recovery in tight, oil-wet reservoirs. They concluded that ultra-low IFT systems can alter the phase behavior and flow pattern of fluids in porous media, enhancing oil recovery. During imbibition, the ultra-low IFT systems promote oil dispersion through emulsification, with the oil phase diffusing out of the porous medium as MEs. Additionally, tiny oil droplets at ultra-low IFT may agglomerate into larger oil droplets due to buoyancy. Using a microscopic model, Yu et al. (2021) investigated the relationship between the imbibition kinetics of MEs and wettability, phase behavior, IFT, and salinity. They revealed that surfactant diffusion plays a crucial role in the imbibition process of ultra-low IFT, aiding in the in-situ formation of MEs and the dilution of high-viscosity MEs. Compared to conventional surfactant imbibition, surfactant molecules capable of forming MEs can solubilize different oil films on the pore surfaces through boundary layer diffusion, completely altering the reservoir wettability and enhancing the imbibition rate and depth. Therefore, it is essential to investigate the influence of solid-liquid interface characteristics of surfactant systems on the imbibition behavior of tight/shale reservoirs, which can provide theoretical guidance for the optimal design of enhanced recovery through imbibition. In this paper, three different imbibition systems are first constructed with distinct interfacial characteristics. Then, systematic analyses are conducted on interfacial interactions, experimental data and numerical simulations. Finally, the relationship between imbibition mechanisms and solid-liquid interfacial behavior in tight/shale reservoirs is clarified.

2. Experimental methodology

2.1 Materials

2.1.1 Fluids

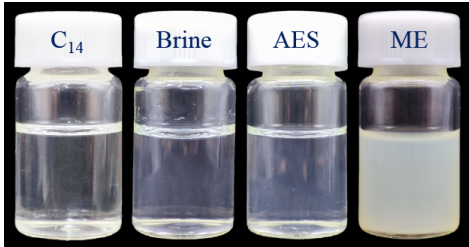
The experimental oil used in this study was tetradecane of analytical purity. Analytically pure compounds such as petroleum sulfonate (KPS), aliphatic alcohol (APS), and fatty alcohol polyoxyethylene ether sodium sulfate (AES, with a mass fraction of 70.0 wt%) were employed in the experiment. All chemicals were supplied by Chengdu Kelon Chemical Co. Three types of imbibition fluids were prepared for this study:

Table 1. Basic physical properties of tetradecane and imbibition fluids (44 °C).

Fluids	Content of NaCl (wt%)	Density (g/cm ³)	Viscosity (cp)	pH	Appearance
Tetradecane	/	0.76	1.1	/	Colorless and transparent
AFS	5.5	1.05	1.0	7.0	Colorless and transparent
AES	5.5	1.05	1.0	7.0	Colorless and transparent
ME	5.5	1.07	1.0	7.0	Milky white and opaque

Table 2. Basic physical properties of the cores.

Cores	Length (cm)	Diameter (cm)	Porosity (%)	Permeability (mD)	Pore volume (cm ³)
A1	4.98	3.82	10.9	0.102	6.22
A2	4.98	3.82	10.4	0.095	5.93
A3	5.00	3.82	10.6	0.096	6.07

**Fig. 1.** Images of tetradecane and the imbibition fluids.

(i) brine (NaCl, 5.5 wt%) serving as a control; (ii) AES, surfactant solution prepared from brine (0.2 wt%); and (iii) ME, surfactant solution capable of forming MEs in situ (KPS and APS mixture, 0.4 wt%). Fig. 1 illustrates the images of tetradecane and the three imbibition fluids. The fundamental physical parameters are provided in Table 1. The imbibition fluids exhibited a density ranging from 1.05 to 1.07 g/cm³ and a viscosity of 1.0 cp.

2.1.2 Tight/shale core samples

Samples A1 to A3 are tight sandstone cores from the Chang 7 formation with permeabilities of 0.1 mD. The basic physical parameters of the cores are presented in Table 2. The cores were aged at 44 °C before testing, and they were saturated to over 98% by tetradecane.

2.2 Methods

2.2.1 IFT measurement

The IFT between different imbibition fluids and tetradecane was measured using a spinning drop tensiometer (Bowling, Stafford, TX 500C) at 44 °C and 6,000 rpm.

2.2.2 Wettability measurement

The efficacy of several imbibition fluids in improving the core wettability was evaluated using a contact angle tester (DSA 25, KRÜSS, Germany). The following steps were performed: (i) The core sample was sectioned, polished with sandpaper and sequentially cleaned with toluene and methanol. (ii) The core sections were aged in brine for three days,

followed by exposure to tetradecane for 28 days, both at a temperature of 44 °C. (iii) After drying and placing the core sections in a testing chamber, brine was introduced to submerge the sections. Subsequently, 4 L of tetradecane was released at the bottom of the sections using a capillary needle, and images of droplets were captured after a 30-minute equilibration period. The test was repeated five times with different droplet release points, and the results were averaged to minimize the influence of surface non-homogeneity. (iv) The core sections were immersed in different imbibition solutions for 7 days at 44 °C. Step (iii) was repeated to compare the alteration in wettability of the core surface (Tagavifar et al., 2019).

2.2.3 Phase behavior test

Three screw-top test tubes containing equal volumes of imbibition fluids and tetradecane were tightly sealed and inverted several times to ensure thorough mixing of the oil and water phases. The tubes were then placed in a 44 °C oven and shaken daily for a period of 7 days. After 14 days, the tubes were removed, and the phase type, phase volume and appearance of the aqueous phase were recorded to evaluate the solubilization performance of the imbibition fluids (Healy et al., 1976; Southwick et al., 2020). The extent of oil and water solubilization (s_o , s_w) per unit volume of surfactant (Healy et al., 1976) are respectively expressed as:

$$s_o = \frac{V_o}{V_s} \quad (1)$$

$$s_w = \frac{V_w}{V_s} \quad (2)$$

2.2.4 Imbibition experiments

Spontaneous imbibition experiments were performed using the gravimetric method. The specific steps were as follows: (i) The core samples were cleaned with toluene and methanol, and then subjected to ultrasonic cleaning. After drying in an oven at 120 °C for one day, the cores were weighed. (ii) The cores were placed in a vacuum saturation apparatus and evacuated to a pressure of 10⁻⁹ Pa. After a 2-day evacuation period, te-

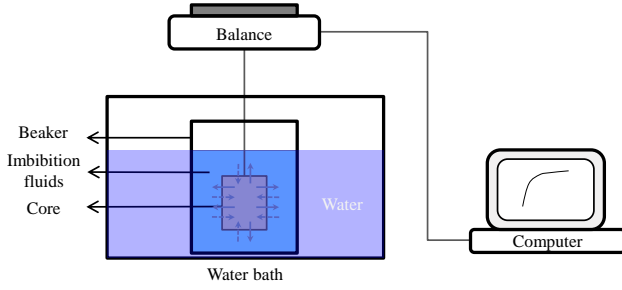


Fig. 2. Schematic diagram of the imbibition experimental device.

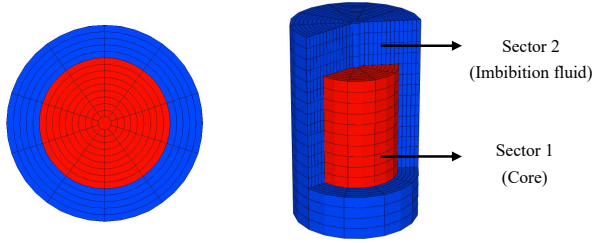


Fig. 3. Schematic of the core spontaneous imbibition model.

tridecane was injected into the core chamber, which was pressurized to 30 MPa and allowed to saturate for 7 days. The volume of saturated oil and oil saturation level were calculated based on the post-saturation core weight. (iii) The cores were immersed in tetradecane for 28 days at 44 °C. (iv) The imbibition test setup, as shown in Fig. 2, was assembled with a constant water bath temperature of 44 °C. The aged cores were removed, dried and immediately submerged in a beaker filled with the imbibition solution. The core mass was recorded at regular intervals until it reached equilibrium and no longer changed. The dynamic imbibition pattern is characterized by the imbibition recovery factor (R_f), which can be determined by:

$$R_f = \frac{\Delta m}{V \Delta \rho} \times 100\% \quad (3)$$

2.3 Numerical simulation

2.3.1 Core model

A radial grid model was constructed using CMG-STARs software for numerical simulation, as shown in Fig. 3. The red section represents the core, whereas the blue section represents the imbibition fluid. Table 3 presents the parameters of the established core model. The details of this model can be found in our previous study (Wei et al., 2023).

2.3.2 Relative permeability and capillary pressure curves

The relative permeability curves were determined using the Brooks-Corey model, as depicted by:

$$K_{rj} = K'_{rj} \left(\frac{S_j - S_{jr}}{1 - S_{wr} - S_{or}} \right)^{n_j} \quad (4)$$

The capillary pressure could be expressed using the power-law model given as (Zhang et al., 2017):

Table 3. Physical parameters of the imbibition model.

Parameter	Value
Model dimension ($r \times \theta \times z$) (cm)	$2.85 \times 360^\circ \times 9$
Number of grid blocks ($r \times \theta \times z$)	$15 \times 10 \times 18$
Porosity (Sector 1) (-)	0.10
Permeability (Sector 1) (mD)	0.1
Oil saturation (Sector 1) (-)	0.9
Porosity (Sector 2) (-)	0.99
Permeability (Sector 2) (D)	10
Water saturation (Sector 2) (-)	0.999
Molecular weight (Tetradecane) (g/mol)	198.39

$$P_c(S_w) = P_{c0} \left(\frac{1 - S_w - S_{or}}{1 - S_{wr} - S_{or}} \right)^{n_c} \quad (5)$$

Wettability affects the shape of the relative permeability curves. The associate relative permeability and contact angle were respectively given by (Kathel and Mohanty, 2013):

$$K'_{rj} = K_{r,w}^o + \frac{\cos \theta_j - \cos \theta_o}{\cos(\pi - \theta_o) - \cos \theta_o} (K_{r,nw}^o - K_{r,w}^o) \quad (6)$$

$$n_j = n_w + \frac{\cos \theta_j - \cos \theta_o}{\cos(\pi - \theta_o) - \cos \theta_o} (n_{nw} - n_w) \quad (7)$$

Moreover, the influence of contact angle and IFT on capillary pressure could be described as:

$$P_c = P_{c0}(S_w) \frac{\sigma \cos \theta}{\sigma_o \cos \theta_o} \quad (8)$$

2.3.3 Modeling wettability alteration

The relationship between adsorption and surfactant concentration in STARS was determined using the Langmuir isotherm adsorption model (Langmuir, 1918). This relationship was utilized as a weight coefficient for wettability alteration during the interpolation of relative permeability curves:

$$\delta = \frac{aC_s}{1 + bC_s} \quad (9)$$

In the model, the lower limit (δ_o^L , usually zero) and upper limit (δ_w^U) of the adsorption capacity corresponds to the relative permeability curves of the initial condition and the final relative permeability curve after wettability modification, respectively. The weight coefficient of wettability alteration was defined as:

$$\omega = \frac{\frac{1}{\delta - \delta_o^L + \varepsilon} - \frac{1}{\varepsilon}}{\frac{1}{\delta_w^L - \delta_o^L + \varepsilon} - \frac{1}{\varepsilon}} \quad (10)$$

Based on the wettability measurement and the adsorption fitting in our previous study (Wei et al., 2023), the relative permeability and capillary pressure within the specified range was calculated by the defined interpolation (Wijaya and Sheng, 2020):

$$K_{rj} = K_{rj,o} + \omega(K_{rj,w} - K_{rj,o}) \quad (11)$$

$$P_c = P_{c,o} + \omega(P_{c,w} - P_{c,o}) \quad (12)$$

2.3.4 Modeling IFT reduction

Alakbarov and Behr (2019) reported that the capillary number, a dimensionless parameter representing the ratio of viscous force to interfacial force, is commonly used in CMG-STARS to simulate IFT reduction:

$$N_c = \frac{\mu v}{\sigma} \quad (13)$$

In this study, the capillary number was replaced by the concentration of ME, a crucial parameter for interpolating relative permeability, which indicates IFT reduction. The lower and upper limits of ME concentration corresponded to the relative permeability profiles for the initial IFT and ultra-low IFT states, respectively. The values of K_r and P_c within the interpolation parameter range were obtained through interpolation by:

$$K_{rj} = (1 - \gamma)K_{rj}^A + \gamma K_{rj}^B \quad (14)$$

$$P_c = (1 - \gamma)P_c^A + \gamma P_c^B \quad (15)$$

Where the interpolation parameter is defined as:

$$\gamma = \left(\frac{x_{ME} - x_A}{x_B - x_A} \right)^n \quad (16)$$

The S_{or} for different IFT levels could be calculated by:

$$S_{or} = (1 - \gamma)S_{or}^A + \gamma S_{or}^B \quad (17)$$

2.3.5 Modeling solubilization and emulsification

When the concentration of surfactants in a solution exceeds the critical micelle concentration, or when the IFT is reduced to an extremely low level, oil solubilization and emulsification occurs (Zhang et al., 2009). Due to droplet diffusion, the newly formed nano-sized oil droplets are transported towards the core surface (Liu et al., 2020). These processes are governed by the following three sequential modes.

2.3.6 Liquid/Liquid K-value

The phase equilibrium constant (K -value), shown as Eq. (18), is defined as the ratio of the mole fraction of a component in a non-reference phase to that of a reference phase at a given temperature and pressure. Herein, by correlating the concentration of ME to oil-water K -values, the effect of oil solubilization was quantified, as given by:

$$K_i^{ow} = \frac{\chi_i^o}{\chi_i^{Bw}} \quad (18)$$

Among them, $K_W^{ow}, K_{ME}^{ow} = 0$, $K_o^{ow} = 1/\chi_{oil}^w$.

2.3.7 Emulsifying kinetics

An emulsifying kinetics was integrated into the modeling to characterize the emulsification reaction between the model oil and ME, as given by:

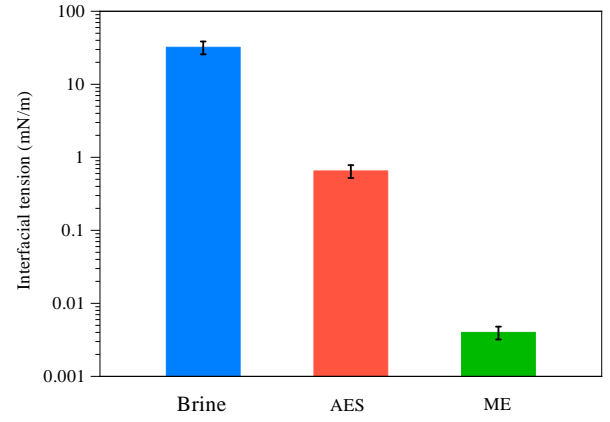
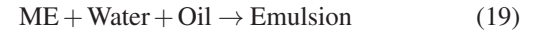


Fig. 4. IFT between different imbibition fluids and tetradecane.



The Arrhenius equation was implemented to determine the reaction rate of all phases and components:

$$r_i = r_{rk} \prod_{i=1}^m C_i^{m_i} \exp\left(-\frac{E_a}{RT}\right) \quad (20)$$

$$C_i = \phi \rho_j S_j \chi_{ji} \quad (21)$$

During the imbibition process, the emulsification rate is mainly governed by the kinetic constant and reaction order. In this study, the reaction order of the reactants was assumed to be 1, indicating that the reaction rate was directly proportional to the concentration. The kinetic constant was treated as an adjustable parameter to match the historical data.

2.3.8 Diffusion of oil droplets

The diffusive behavior of the formed oil particles is characterized by the Stokes-Einstein equation:

$$D = \frac{\kappa T}{6\pi\mu r} \quad (22)$$

3. Results and discussion

3.1 IFT between imbibition fluids and model oil

The IFT between the three imbibition fluids and tetradecane reflects the magnitude differences, as shown in Fig. 4. The IFT between brine and tetradecane is 32 mN/m. AES can reduce the IFT to the range of 10^{-1} mN/m, while ME can achieve an ultra-low IFT level in the range of 10^{-3} mN/m. The observed gradient variations in IFT met the requirements of this study in terms of imbibition fluids with diverse oil-water interface properties.

3.2 Wettability alteration

The wettability test results for the core samples before and after immersion in different imbibition fluids are presented in Fig. 5. Initially, all contact angles of the tetradecane-aged core samples were greater than 90° , indicating a neutral-wet or oil-wet state. Following a 7-day treatment with AES and ME, the equilibrium contact angles were less than 90° , indicating a water-wet condition. Notably, ME exhibited strong water-

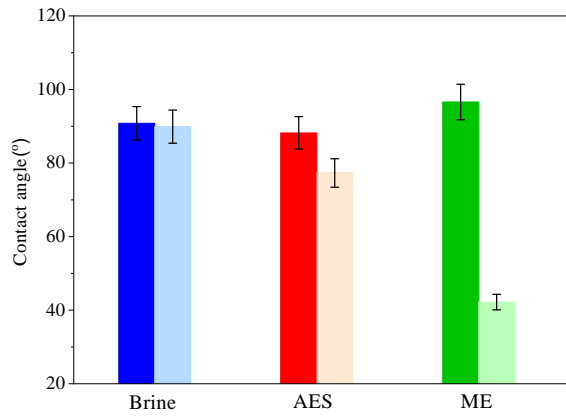


Fig. 5. Core wettability before and after treatment with different imbibition fluids.

wet behavior, with a contact angle of 42.2° . This significant wettability alteration could be attributed to the exceptional solubilization capacity of ME, which effectively removed the adsorbed oil film from the rock surface. In contrast, traditional surfactant AES primarily relies on surface adsorption to enhance wettability.

3.3 Phase behavior between imbibition fluids and model oil

The results of the oil-aqueous phase behavior tests conducted with different imbibition fluids are illustrated in Fig. 6, with selected images taken at 1, 7 and 14 days, respectively. The position of the first oil-water contact is indicated on the 5 mL scale of the test tube. The graphs show that after 14 days of contact between surfactant AES and tetradecane, there were no significant changes in the phase type, phase volume or appearance of the aqueous phase compared to the initial state at 1 day, indicating that the AES did not solubilize tetradecane. In contrast, after 14 days of contact with tetradecane, ME formed a stable triple phase in the test tube, with both the aqueous phase (lower phase) and the oil phase (upper phase) appearing colorless and transparent. The phase test results revealed that when the oil-water interfacial tension was reduced to 10^{-3} mN/m, there was a significant alteration in the oil-aqueous phase behavior, indicating an increased interfacial activity of the imbibition fluids and their enhanced solubilization capacity.

3.4 Imbibition oil recovery

The relationship between the interface characteristics of the imbibition fluid and the ultimate recovery is shown in Table 4.

The imbibition recovery profiles of the three imbibition fluids over time are illustrated in Fig. 7. ME exhibits the highest imbibition recovery rate, reaching 36.5%, followed by AES at 16.2% and brine at only 5.0%. As shown in Fig. 5, the core surfaces display lipophilic characteristics and are resistant to imbibition due to tetradecane aging. The immersion treatment with brine did not significantly improve the core surface wettability. At a high IFT of 32 mN/m, the aqueous phase experienced significant imbibition resistance. However,

due to the non-uniform wettability distribution, a small amount of brine still managed to enter the core, resulting in a relatively low overall imbibition recovery.

AES has the capability to reduce the oil-water IFT to 0.65 mN/m, significantly decreasing the capillary resistance encountered by the aqueous phase during entry into the core. This reduction allows the aqueous phase to penetrate macropores in the core under the influence of gravity. Upon entry, the surfactant molecules facilitate a wettability alteration of the core surface, transitioning it to weak water wetting through surface adsorption (Fig. 5). The capillary force is thereby converted into imbibition power, resulting in a substantial enhancement of the imbibition recovery rate. The IFT between ME and tetradecane is extremely low (10^{-3} mN/m), resulting in negligible resistance for the aqueous phase to penetrate the core. Through boundary layer diffusion, ME exhibits the spontaneous solubilization of oil films on various pore surfaces, leading to a significant enhancement of core wettability (Liu et al., 2022). Concurrently, the diffusion of surfactant into the oil phase at the imbibition front induces a temporary decrease in surfactant concentration in the aqueous phase, leading to an increase in oil-water IFT and capillary force. This augmentation facilitates the continuation of imbibition. The subsequent influx of the aqueous phase continuously replenishes the surfactant at the imbibition front, maintaining a dynamic process of capillary force, which serves as the driving force for imbibition. Our previous study has confirmed the validity of this mechanism (Wei et al., 2023). The time-dependent change in the imbibition rate of the core can provide further insights into the relationship between the characteristics of the solid-liquid interface and imbibition behavior. The imbibition rate was calculated using the following equation:

$$v_i = 3600 \times \frac{\Delta m}{A_c t \Delta \rho} \quad (23)$$

The variation pattern of the imbibition rate for different imbibition fluids is shown in Fig. 8. During the initial stage of imbibition, the capillary forces dominate the resistance, and the entry of the aqueous phase into the core is primarily driven by gravity. Lower IFT values correspond to lower capillary resistance, resulting in a higher imbibition rate. Therefore, ME with its ultra-low IFT exhibits the maximum imbibition rate during the early phase. The imbibition rate is positively correlated with the hydrophilicity of the core. ME shows a dynamic change in IFT at the leading edge of imbibition, leading to a stable imbibition rate over a specific time period. On the other hand, AES has limited ability to enhance wettability, resulting in an extremely low imbibition rate. In the later stages of imbibition, the available pore substrates shift from larger pores to smaller and medium-sized ones, causing an increase in flow resistance, a decrease in oil saturation, and a higher imbibition difficulty. While all three imbibition fluids exhibit a decreasing trend in their imbibition rates, the imbibition rate of ME remains the highest due to its strong interfacial activity.

3.5 Numerical simulation

In order to validate the applicability of our proposed imbibition simulation approach, a numerical model was developed

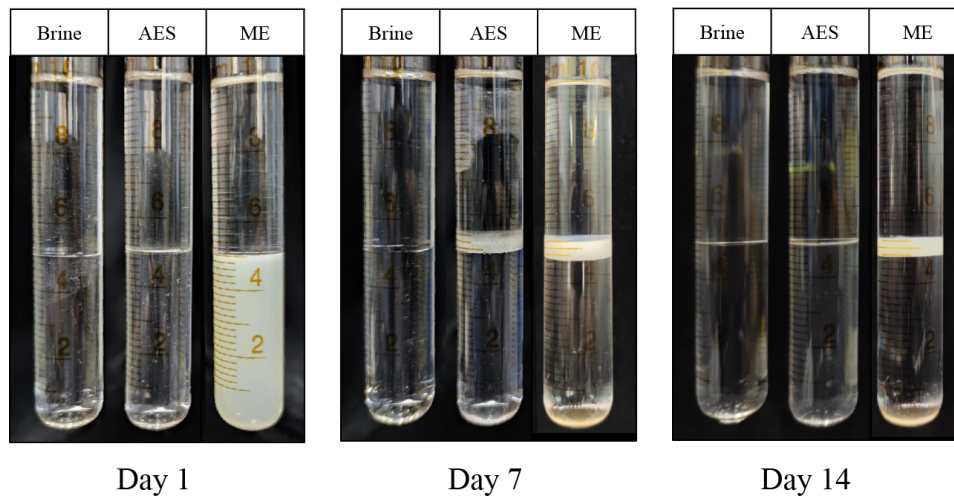


Fig. 6. Oil-aqueous phase behaviors of different imbibition fluids.

Table 4. Interfacial characteristics and imbibition recovery of different imbibition fluids (44 °C).

Core	Fluid	Oil saturation (%)	IFT (mN/m)	Contact angle (°)	s_o	s_w	Ultimate recovery (%)
A1	Brine	89.6	32.010	88.0	/	/	5.1
A2	AES	91.0	0.650	73.3	/	/	16.2
A3	mE	90.8	0.004	42.2	8.8	8.8	36.5

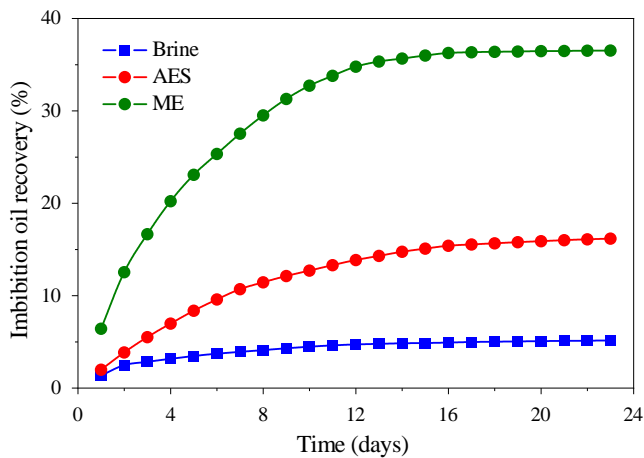


Fig. 7. Changes in the imbibition recovery of different imbibition fluids with time.

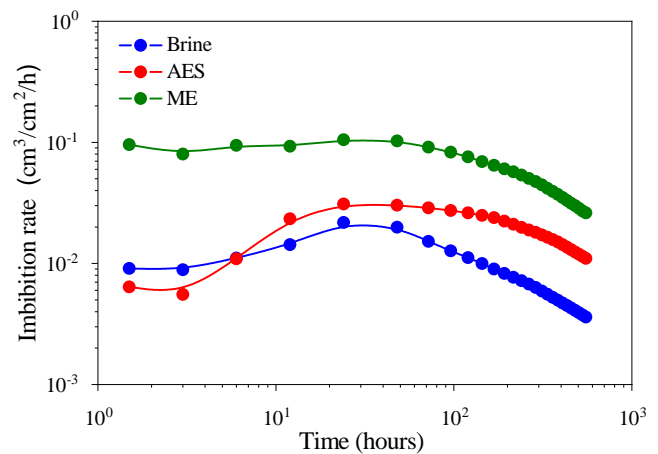


Fig. 8. Variation in the imbibition rate of different imbibition fluids with time.

to match the experimental results of brine, AES and ME imbibition. Based on the findings from the physiochemical properties of imbibition fluids, distinct mechanisms were considered for AES and ME. AES accounted for wettability alteration and IFT reduction, while ME additionally accounted for solubilization and emulsification. By continuously adjusting the endpoint values and exponents of the relative permeability and capillary pressure curves, history-matching for brine imbibition was straightforward. The initial values of K_r and P_r for AES and ME imbibition were derived from brine imbibition experiments and the final values were calculated using the equations. The contrast between the experimental and simulated outcomes is presented in Fig. 9, while Table 5

lists the relevant parameters for the history matching of the imbibition experiments. Table 6 displays the optimal parameter settings for ME in the model. It is evident that the experimental and simulation results exhibit a high degree of fitting accuracy. In contrast to AES, ME not only alters wettability and decreases IFT but also participates in the emulsification reaction and is consistently consumed. In our model, the emulsification reaction is assumed to be rapid and continuous. The enhanced imbibition efficacy of ME is evident in terms of oil recovery factor and rate. It was conjectured that the diffusion, spontaneous emulsification, and wettability alteration of ME all accelerate the imbibition process (Wei et al., 2021).

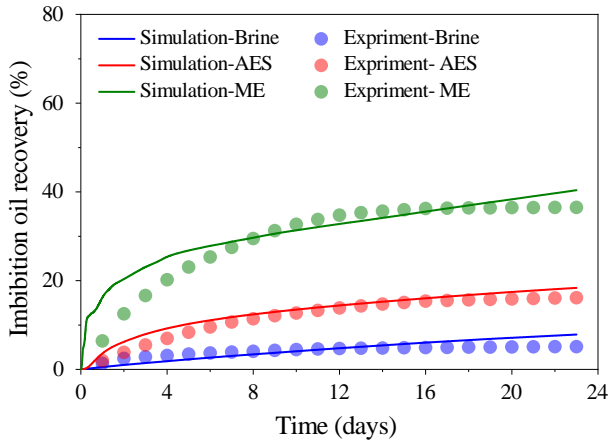


Fig. 9. Imbibition oil recovery of experimental results and simulation data.

Table 5. Related parameters of the imbibition models.

Parameter	Brine	AES	ME
S_{or} (-)	0.25	0.25	0.25
S_{wi} (-)	0.1	0.1	0.1
K_{rw} (-)	0.72	0.67	0.59
K_{ro} (-)	0.72	0.77	0.85
n_w (-)	4.3	5.4	7.0
n_o (-)	4.4	3.3	1.7
P_{c0} (kPa)	-10.50	14.29	202.63
n_c (-)	6	6	6

4. Conclusions

- 1) With the highest imbibition recovery and possessing ultra-low interfacial tension and solubilization capacity, ME can effectively reduce the flow resistance and significantly improve the rock surface wettability.
- 2) Interfacial diffusion induces a decline in the concentration of ME near the imbibition front, leading to dynamic variations in interfacial tension and capillary force, thereby facilitating the advancement of imbibition.
- 3) Numerical simulation demonstrates that solubilization and emulsification play pivotal roles in ME imbibition. This process results in higher oil recovery and faster recovery rate compared to other imbibition fluids.
- 4) A system characterized by high interfacial activity, such as ME, justifies further research for imbibition processes in unconventional reservoir formations.

Nomenclature

a, b = adsorption constants
 A, B = upper and lower limits of ME concentration
 A_c = core surface area
 C_S = mole fraction of surfactants in aqueous phase
 C_i = concentration factor of reactant i

Table 6. Parameter setting for the history matching of the ME imbibition experiment.

Parameter	Value
r_{rk} (emulsification) (-)	40,000
r_{rk} (demulsification) (-)	10,000
Oil droplets diffusion (cm^2/min)	2.62×10^{-6}
Exponent- K_{ro} (-)	2
Exponent- K_{rw} (-)	2
Exponent- P_{cow} (-)	2

D = diffusion coefficient of oil droplets
 E_a = activation energy
 i = oil, water or ME
 j = oil or water
 K_i^{ow} = phase equilibrium constant of component i in oil and water
 K_{rj} = relative permeability of phase j
 K_{rj}^l = endpoint value of the relative permeability of phase j
 $K_{r,w}^0$ = endpoint on initial relative permeability of wetting phase
 $K_{r,nw}^0$ = endpoint on initial relative permeability of non-wetting phase
 K_{rj} = relative permeability of phase j
 $K_{rj,o}, K_{rj,w}$ = relative permeability of oil- and water-wet states
 $K_{rj}^i (K_{rw}^A, K_{rw}^B, K_{ro}^A, K_{ro}^B)$ = relative permeability curves corresponding to x_A and x_B
 m = total number of reactants
 m_i = reaction order of reactant i
 n = exponent of weight coefficient for IFT reduction
 n_j = exponent of phase j
 n_c = exponent of capillary pressure curve
 n_{wet}, n_{nw} = exponent of relative permeability of wetting/non-wetting phases
 N_c = capillary number
 P_c = capillary pressure
 P_{c0} = endpoint value of capillary pressure curve
 $P_{c,o}, P_{c,w}$ = capillary pressure curves of oil- and water-wet states
 $P_c^i (P_c^A, P_c^B)$ = capillary pressure curves corresponding to x_A and x_B
 r = radius of oil droplets
 r_i = reaction rate of component i
 r_{ik} = kinetic constant
 R = Avogadro constant
 R_f = imbibition recovery factor
 S_j = saturation of phase j
 S_{jr} = residual saturation of phase j
 $S_{or}^i (S_{or}^A, S_{or}^B)$ = residual oil saturation corresponding to x_A and x_B
 s_o, s_w = solubilization parameters of oil, water
 t = imbibition rate
 T = temperature

v_i = imbibition rate
 V = oil content of cores
 V_o, V_w, V_s = volume of oil/water/surfactant in ME phase
 χ_i = molar fraction of ME
 χ_A, χ_B = mole fraction of ME at initial/ultralow IFT states
 χ_{ji} = mole fraction of component i in j phase
 χ_i^o, χ_i^w = mole fraction of component i in oil or water
 Δm = mass changes of cores in imbibition fluids
 $\Delta \rho$ = density difference between oil and exudate
 θ_0 = initial contact angle
 θ_j = contact angle of phase j
 δ = isothermal adsorption of surfactant
 ω = weight coefficient of wettability alteration
 δ_o^L = lower boundary of adsorption capacity at initial oil-wet state
 δ_w^u = upper boundary of adsorption capacity at final water-wet state
 ϵ, τ = curvature parameter and curve-fitting exponent for K_r and P_c
 σ = IFT
 σ_0 = initial IFT
 γ = weight coefficient for IFT reduction
 Φ = porosity
 ρ_j = density of phase j
 κ = Boltzmann constant
 μ = fluid viscosity

Acknowledgements

The authors gratefully acknowledge the financial support of the National Natural Science Foundation of China (No. 52274041), and the Sichuan Science Fund for Distinguished Young Scholars (No. 2023NSFSC1954). The authors also thank the Computer Modeling Group Ltd. for providing the CMG software for this study, and the McDougall School of Petroleum Engineering (The University of Tulsa).

Conflict of interest

The authors declare no competing interest.

Open Access This article is distributed under the terms and conditions of the Creative Commons Attribution (CC BY-NC-ND) license, which permits unrestricted use, distribution, and reproduction in any medium, provided the original work is properly cited.

References

- Alakbarov, S., Behr, A. Evaluation of surfactant application to increase oil recovery in bottom aquifer-driven naturally fractured reservoir. Paper SPE 196615 Presented at SPE Reservoir Characterisation and Simulation Conference and Exhibition, Abu Dhabi, 17-19 September, 2019.
- Bu, X., Han, M., Alsofi, A. M. Core-scale modeling of surfactant-assisted spontaneous water imbibition in carbonates. *Petroleum*, 2022, 8(4): 458-465.
- Cai, J., Chen, Y., Liu, Y., et al. Capillary imbibition and flow of wetting liquid in irregular capillaries: A 100-year review. *Advances in Colloid and Interface Science*, 2022, 304: 102654.
- Cai, J., Hu, X., Standnes, D. C., et al. An analytical model for spontaneous imbibition in fractal porous media including gravity. *Colloids and Surfaces A: Physicochemical and Engineering Aspects*, 2012, 414: 228-233.
- Cai, J., Jin, T., Kou, J., et al. Lucas-Washburn equation-based modeling of capillary-driven flow in porous systems. *Langmuir*, 2021, 37(5): 1623-1636.
- Cao, Y., Tang, M., Zhang, Q., et al. Dynamic capillary pressure analysis of tight sandstone based on digital rock model. *Capillarity*, 2020, 3(2): 28-35.
- Chen, P., Mohanty, K. K. Surfactant-mediated spontaneous imbibition in carbonate rocks at harsh reservoir conditions. *SPE Journal*, 2013, 18(1): 124-133.
- Cheng, X., Kleppe, J., Torsaeter, O. Simulation study of surfactant imbibition mechanisms in naturally fractured reservoirs. Paper SPE 191309 Presented at SPE Norway One Day Seminar, Bergen, Norway, 18 April, 2018.
- Healy, R. N., Reed, R. L., Stenmark, D. Multiphase microemulsion systems. *Society of Petroleum Engineers Journal*, 1976, 16(3): 147-60.
- Kathel, P., Mohanty, K. K. Wettability alteration in a tight oil reservoir. *Energy & Fuels*, 2013, 27(11): 6460-6468.
- Langmuir, I. The adsorption of gases on plane surfaces of glass, mica and platinum. *Journal of the American Chemical Society*, 1918, 40(9): 1361-1403.
- Li, Y., Pope, G. A., Lu, J., et al. Scaling of low-interfacial-tension imbibition in oil-wet carbonates. *SPE Journal*, 2017, 22(5): 1349-1361.
- Liang, Y., Lai, F., Dai, Y., et al. An experimental study of imbibition process and fluid distribution in tight oil reservoir under different pressures and temperatures. *Capillarity*, 2021, 4(4): 66-75.
- Lin, H., Zhang, S., Wang, F., et al. Experimental investigation on imbibition-front progression in shale based on Nuclear Magnetic Resonance. *Energy & Fuels*, 2016, 30(11): 9097-9105.
- Liu, D., Xu, J., Zhao, H., et al. Nanoemulsions stabilized by anionic and non-ionic surfactants for enhanced oil recovery in ultra-low permeability reservoirs: Performance evaluation and mechanism study. *Colloid Surface A: Physicochemical and Engineering Aspects*, 2022, 637: 128235.
- Liu, J., Sheng, J., Tu, J. Effect of spontaneous emulsification on oil recovery in tight oil-wet reservoirs. *Fuel*, 2020, 279: 118456.
- Lu, J., Goudarzi, A., Chen, P., et al. Enhanced oil recovery from high-temperature, high-salinity naturally fractured carbonate reservoirs by surfactant flood. *Journal of Petroleum Science and Engineering*, 2014, 124: 122-131.
- Ma, Q., Zhu, W., Bu, W., et al. Pore-scale imbibition comparisons between capillary and gravity forces reveal distinct drainage mechanisms and residual oil distributions. *Colloids and Surfaces A: Physicochemical and Engineering Aspects*, 2022, 653: 129981
- Mason, G., Morrow, N. R. Developments in spontaneous imbibition and possibilities for future work. *Journal of Petroleum Science and Engineering*, 2013, 110: 268-293.
- Mejia, L., Tagavifar, M., Xu, K., et al. Surfactant flooding in oil-wet micromodels with high permeability fractures.

- Fuel, 2019, 241: 1117-1128.
- Neog, A., Schechter, D. S. Investigation of surfactant induced wettability alteration in wolfcamp shale for hydraulic fracturing and EOR applications. Paper SPE 179600 Presented at SPE Improved Oil Recovery Conference, Tulsa, Oklahoma, USA, 11-13 April, 2016.
- Pi, Z., Peng, H., Jia, Z., et al. mechanisms of displacement and imbibition in pore-fracture system of tight oil reservoir. *Capillarity*, 2023, 7(1): 13-24.
- Saravanan, S., Keerthana, S. Floquet instability of gravity-modulated salt fingering in a porous medium. *Industrial & Engineering Chemistry Research*, 2017, 56(10): 2851-2864.
- Southwick, J. G., Van, R. C., Van, D. P. E., et al. Advantages of an APS/AES seawater-based surfactant polymer formulation. *SPE Journal*, 2020, 25(6): 3494-3506.
- Tagavifar, M., Balhoff, M., Mohanty, K., et al. Dynamics of low-interfacial-tension imbibition in oil-wet carbonates. *SPE Journal*, 2019, 24(3): 1092-1107.
- Wei, B., Mao, R., Tang, H., et al. Facile fabrication of nanoemulsions through the efficient cationic surfactants for spontaneous imbibition in tight oil reservoirs: Experimental and numerical simulation. Paper SPE 204336 Presented at SPE International Conference on Oilfield Chemistry, The Woodlands, Texas, USA, 6-7 December, 2021.
- Wei, B., Wang, L., Mao, R., et al. Understanding imbibition mechanisms of cationic surfactant-stabilized nanoemulsion for enhanced oil recovery in tight sandstone reservoirs: experimental and numerical assessment. *SPE Journal*, 2023, 28(3): 1437-1452.
- Wijaya, N., Sheng, J. Mitigating near-fracture blockage and enhancing oil recovery in tight reservoirs by adding surfactants in hydraulic fracturing fluid. *Journal of Petroleum Science and Engineering*, 2020, 185: 106611.
- Yu, F., Gao, Z., Zhu, W., et al. Experiments on imbibition mechanisms of fractured reservoirs by microfluidic chips. *Petroleum Exploration and Development*, 2021, 48(5): 1162-1172.
- Zhang, J., Bi, H., Xu, H., et al. New progress and reference significance of overseas tight oil exploration and development. *Acta Petrolei Sinica*, 2015, 36(2): 127-137. (in Chinese)
- Zhang, J., Nguyen, Q. P., Flaaten, A. K., et al. Mechanisms of enhanced natural imbibition with novel chemical. *SPE Reservoir Evaluation & Engineering*, 2009, 12(6): 912-920.
- Zhang, Y., Fan, Z., Yang, D., et al. Simultaneous estimation of relative permeability and capillary pressure for PUNQ-S3 model with a damped Iterative-Ensemble-Kalman-Filter technique. *SPE Journal*, 2017, 22(3): 971-984.
- Zhou, Y., Guan, W., Zhao, C., et al. Spontaneous imbibition behavior in porous media with various hydraulic fracture propagations: A pore-scale perspective. *Advances in Geo-Energy Research*, 2023, 9(3): 185-197.